Accepted version of Schwarz et al. Scripta Materialia 232 (2023) 115498

Uncovering Ce-rich clusters and their role in precipitation strengthening of an AE44 alloy

Tim M. Schwarz[1], Wenhao Yu[2], Hongyi, Zhan[3], Baptist Gault[1,2], Christopher M. Gourlay[2], Ingrid McCarroll[1, *]

1. Max-Planck-Institut für Eisenforschung, Max-Planck-Str. 1, Düsseldorf 40237, Germany
2. Department of Materials, Imperial College London, London, SW7 2AZ, UK
3. China Science Lab, General Motors Global Research and Development, Shanghai, 201206, China

*Corresponding author E-mail address: i.mccarroll@mpie.de, tim.schwarz@mpie.de

ORCID:

Tim M. Schwarz: https://orcid.org/0000-0001-9348-4160

Baptist Gault: https://orcid.org/0000-0002-4934-0458

Christopher Gourlay: https://orcid.org/0000-0002-4588-6007

Ingrid McCarroll: https://orcid.org/0000-0002-0584-4769

Keywords: magnesium, AE44, aging, precipitation, atom probe tomography

Abstract

The peak-aged (250°C for 4h) Magnesium-aluminum-rare earth (Mg-Al-RE) alloy AE44-2 produced using high-pressure die casting, exhibits a 10 % increase in yield strength attributed to the formation of nanoscale AlMn precipitates. Here, in the as cast state, we show by atom probe tomography Ce-rich clusters in the dendritic and not in the inter-dendritic α-Mg, despite a higher RE concentration. Their formation hence depends mainly on solidification kinetics and not on the concentration. The Ce-rich clusters within the dendritic region, act as heterogeneous nucleation sites for the formation of $Al_{10}Mn_7RE_2$ nanoscale precipitates during the T5 heat treatment. No changes in the $Al_{11}RE_3$ lamella phase were observed, including to the concentration of segregated Si at the $Al_{11}RE_3$/α-Mg interface. Understanding the precipitate formation pathways, specifically the influence of low concentrations of Ce in the dendritic matrix, provides a pathway for tailoring mechanical properties by manipulating these clusters and consequently precipitation.

Ongoing efforts to reduce energy consumption and greenhouse gas emissions are leading to increased efforts to develop lightweight vehicles. Magnesium alloys are amongst the lightest commercially used engineering materials, and are currently used across the automotive, aerospace, and transportation industries [1–5]. However, wide application of magnesium alloys are hindered by low strength and ductility, and poor corrosion resistance and creep behavior [3]. Furthermore, at elevated temperatures, the mechanical properties decrease significantly [6]. In automotive applications, especially for the powertrain, alloys are exposed to temperatures in the range of 150-200 °C. Therefore, Mg-alloys that maintain acceptable mechanical, corrosion, and creep resistant properties at these temperatures are needed [6–8].

Magnesium-aluminum-rare earth (Mg-Al-RE) systems have been developed as high pressure die casting (HPDC) alloys with high strength and good creep behavior, even at elevated temperatures [9–13]. This has been attributed to the formation of Al-RE intermetallic particles, which have high thermal stability [14–16]. Two representatives of these Mg-Al-RE alloys are AE42 and AE44. To suppress the formation of the β-$Mg_{17}Al_{12}$ phase at higher temperatures, which decreases strength and creep resistance, an RE/Al ratio above 3:4 must be maintained. The preferential formation of the $Al_{11}RE_3$ phase [17], makes AE44 a better candidate for application at elevated temperature. Typically, the source of RE is mischmetal, which contain cerium (Ce), lanthanum (La), neodymium (Nd), and praseodymium (Pr). Due to the increased demand of Nd and Pr for magnetic applications [18], Ce and La are the lowest cost RE elements and are preferentially used in AE44 [15,19]. Manganese (Mn) is also a standard addition, used to bind impurity iron in the form of $Al_x(FeMn)_y$ intermetallic phases, increasing the overall corrosion resistance of the alloy [20].

Thermal aging is a standard process used to adjust mechanical properties by precipitation hardening of Mg alloys [21–31]. HPDC AE44 components were initially used in the as-cast condition, as is common with many HPDC components [32], partly because an age hardening response was not expected from an alloy with apparently stable intermetallic that do not dissolve [33]. However, recent work has shown that for HPDC AE44 with minor additions of Mn, a T5 heat treatment leads to significant increase in strength and hardness [33–35]. The strengthening effect was not observed without heat treatment [34] or for alloys without Mn addition [33]. A further addition of Mn did not result in any further increase in strength. Therefore, a critical concentration

of Mn exists [34]. The increase in strength and hardness were attributed to the formation of nanoscale AlMn precipitates on the order of 10 nm based on transmission electron microscopy (TEM) observations [33–37]. However, the precise nature, chemical composition, and precipitation path of these particles has not yet been determined and addressing this knowledge gap could help optimize future Mg-Al-RE alloys.

Here, we use atom probe tomography (APT), which provides a sub-nanometer compositional mapping in 3D [38], to study the chemistry and formation mechanism of precipitates and intermetallic phases in an AE44-2 alloy. The alloy composition is given in Table 1. The RE are derived from a two-component La+Ce mischmetal.

The alloy was cast using an LK-280T cold chamber HPDC machine. The melt was held at 710 °C +/- 10 °C prior to being ladled into a shot sleeve pre-heated to 200 °C and injected into the die preheated to 170 – 190 °C. The plunger speed was set to 0.15 m/s in the slow phase, 3.7 m/s in the fast phase, and the after pressure was set at 100 MPa. Castings were manually removed from the die and quenched in water. The die used produced tensile test bars with gauge length of 50 mm and an 8 mm diameter. Some test bars were kept in the as-cast condition and others were given a T5 heat treatment of 4 hours at 250 °C, followed by quenching in water. As-cast and T5 heat treated bars were tensile tested at room temperature (~20 °C) using an Instron 5982 at a strain rate of 10^{-4} s^{-1}.

The two microstructures, as cast and T5 heat treated, were analysed using a Zeiss Auriga scanning electron microscope (SEM). The samples were ground to 4000 grit SiC paper and afterwards polished with water-free OPS to avoid surface oxidation. To lightly etch the microstructure, samples were immersed in a solution of 200 ml ethylene glycol, 68 ml distilled water, 80 ml acetic acid and 4 ml nitric acid. To deeply etch the α-Mg phase and expose the 3D structure of some intermetallic phases, 10% nitric acid was used.

Based on the development of multiple phases and due to the strong variations of the flow and solidification conditions in the different stages of the HPDC process, a complex microstructure is formed (Figure 1). The backscattered electron micrographs, Figure 1 a–b, feature the characteristic HPDC AE44 microstructure: α-Mg dendrites

(dark regions) surrounded by α-Mg + $Al_{11}RE_3$ lamellar eutectic in the inter-dendritic regions and at grain boundaries (yellow arrows), consistent with previous work [39–41]. Selective etching of the α-Mg in the inter-dendritic region Figure 1 c-d, shows that the $Al_{11}RE_3$ lamellae have a width of approx. 50 nm. There are also much larger blocky Al_2RE particles (red arrows) which are present only in small quantities [40,42] and blocky Mn-containing $Al_{10}Re_2Mn_7$ particles (blue arrows) [33,35,36,43]. These larger particles are normally located at grain boundaries with a typical size of 0.5–4 µm [43].

Tensile curves of six samples from each state are shown in Figure 2. The T5 heat treatment leads to an improvement in yield strength of approx. 10% with comparable elongation, also consistent with previous work [33–35]. Both Al-RE intermetallic phases are thought to be thermally stable, and the proportion of intermetallic phases did not change after the heat treatment (see Figure 1), similar to previous reports of heat treated AE44 alloys [39–41]. Therefore, any changes in strength or hardness are assumed to be attributable to changes in the microstructure at lower length scales, that can be resolved using APT.

Needle-shaped APT specimens were fabricated using a FIB lift-out-based specimen preparation protocol outlined in Thompson et al. [44]. A plasma FIB (FEI Helios PFIB) was used to avoid contamination of the sample by Ga ions since these ions tend to interact strongly with magnesium, as is the case with aluminum [45]. The samples used for APT had not been tensile tested. APT experiments were performed using a Cameca LEAP 5076XS atom probe. Voltage pulsing was used, with a pulse fraction of 20 %, pulse repetition rate of 200-500 kHz, and a detection rate between 1.5-3 %. Data reconstruction was performed using Cameca integrated visualization and analysis software (IVAS) in AP Suite 6.1.

Figure 3 a–b shows the elemental map of Al, Mn, and Ce in the as-cast state and after T5 heat treatment, respectively. Small clusters of Ce are observed in the as cast state, whereas Mn is homogeneously distributed. The size and chemical composition of these clusters and particles were investigated by extracting regions delineated by 0.5 at. % Ce iso-concentration surfaces (Figure 3 c–d). The Ce-rich clusters have a spherical shape with a diameter of 3.3 ± 0.7 nm, and a composition close to Al_2RE, with Ce being the main RE element, and no Mn (Table 2). Typically, intermetallic phases have a higher evaporation field than the Mg matrix, leading to trajectory

aberrations and overestimation of the Mg content in small clusters [46]. Therefore, the Mg signal was excluded from the composition calculation.

After the T5 heat treatment, precipitation of Ce and Mn is visible, Figure 3 b. The spherical particles of approx. 6.7 ± 0.6 nm, are consistent with previous TEM observations by Zhu et al. [33,35], who reported precipitates to be less than 10 nm. In other work, Yang et al. [36] identified precipitates as an intermetallic Al_8Mn_5 phase, due to the rhombohedral structure and crystallographic matching with the α-Mg. They reported that these particles contain traces of RE [36], similar to Li et al. [37], whose energy-dispersive X-ray spectroscopy (EDX) data revealed noticeable signals of Ce, later not included in their reported composition. APT analysis, in contrast, suggests that the composition of these precipitates is $Al_{10}Mn_7RE_2$ (Table 2).

The presence of Ce-rich clusters in the dendritic region of α-Mg in the as cast state was not reported using TEM [33,34,36]. It is proposed that, these Ce-rich clusters likely act as nucleation sites to the manganese-bearing precipitates, i.e. during heat treatment, Mn diffuses and incorporates into these clusters and forms Mn-rich, $Al_{10}Mn_7RE_2$ particles. Lamm et. al. [47] observed a similar phenomenon in a Mg-Ca-based alloy with Al_2Ca clusters in the as cast state. After thermal aging and creep testing at elevated temperatures, Mn was incorporated into the clusters and formed Mn-rich precipitates, leading to an improvement in the mechanical properties. These Mn-rich precipitates contribute to the increase in strength, affecting the dislocation movement, which mainly depends on their coherence and size.

Thermally stable intermetallic phases, in particular $Al_{11}RE_3$, also prevent grain boundary sliding, leading to better creep resistance at elevated temperatures and an increase in strength due to grain boundary reinforcement [41]. The $Al_{11}RE_3$ phase has a lamella structure with a length of several micrometers and a lamella thickness of about 50 nm (see Figure 1 and 4). To understand the influence of heat treatment on the stability of $Al_{11}RE_3$, this inter-dendritic region was also investigated by APT in the as-cast and heat treated states. Figure 4 shows the APT three-dimensional reconstruction of a dataset crossing through an $Al_{11}RE_3$ lamellae in the as-cast state. In the elemental maps of the individual elements, Al, La, and Ce are present in the $Al_{11}RE_3$ phase.

The measured width of the lamellar $Al_{11}RE_3$ phase is approx. 50 nm. The composition of the lamellar phase, determined from a 20 x 20 x 20 nm^3 box positioned in its core, Table 3, is consistent with the $Al_{11}(Ce,La)_3$ phase reported in the literature [33,35,41,48]. The concentration of La, 5.99 at. %, is much higher compared to that observed within the Ce-rich clusters and particles in the α-Mg dendritic region (0.17 at. % La in Table 2). This indicates that La tends to partition mainly in the $Al_{11}RE_3$ phase within the inter-dendritic region, which was also reported by Zhu et al. [40]. No Mn was observed in the $Al_{11}RE_3$ phase. Other impurities such as P and Be were also detected in the lamella phase. A residual Mg concentration of approx. 9.77 at. % is still in the $Al_{11}RE_3$ phase. Previous TEM analyses [49] suggested that small amounts of residual Mg may remain trapped during the formation of the lamella structure, which is confirmed by our analyses.

No discernable change or decomposition of the $Al_{11}RE_3$ phase was observed after the T5 heat treatment (Figure 5). It has been reported, that Mn-rich precipitates form directly on the $Al_{11}RE_3$ phases [36,37], but we did not observe this in the APT analyses. The composition of both intermetallic phases in the heat-treated sample measured by APT is reported in Table 3. These two can be considered as $Al_{11}(Ce,La)_3$ lamellae, yet with different fractions of RE. In the upper lamella, the ratio of Ce to La is 50:50, resulting in an La content approx. 11.56 at. % (Figure 5 and Table 3). In the lower lamella, on the other hand, most of the RE is Ce (Figure 5 and Table 3). Ce and La having similar atomic radii r_{Ce}=182 pm and r_{La}=187 pm and similar valence and electronegativity [48,50] facilitates their substitution by one another.

Table 4 compares the composition of α-Mg in the dendritic and inter-dendritic (i.e. eutectic) regions in the as-cast state. The concentrations of Al and RE increase by a factor of 1.4 and 4.3, respectively, which is attributed to micro segregation due to the low solubility of RE and Al in α-Mg, whereas the concentration of Mn remains similar. In general, the concentration of RE elements in the dendritic α-Mg is assumed to be less than 0.1 at. % due to low solubility in α-Mg [41] and increases in the inter-dendritic α-Mg. However, Ce-rich clusters were found in the dendritic α-Mg which has low RE content (Table 4), and no Ce-rich clusters were observed in the inter-dendritic α-Mg where the concentration of RE is higher. This indicates that the formation of the Ce-rich clusters in α-Mg does not depend mainly on the concentration, but significantly on the solidification kinetics. Therefore, in the future, studies could focus on manipulating

the solidification kinetics to increase the proportion of Ce clusters that subsequently nucleate AlMnRE precipitates to improve the mechanical properties.

Interestingly, the Si content in the inter-dendritic region increases by a factor of 2.1 (Table 4) and Si segregates preferentially at the interface between the lamella $Al_{11}RE_3$ phase and α-Mg. Compositional analysis using a 15-nm-diameter cylinder, positioned across the interface between the $Al_{11}RE_3$ phase and α-Mg, shows approx. 1 at. % Si inside the intermetallic phase, roughly 0 at. % in the α-Mg, and approximately 7 at. % at the interface (Figure 4 and 5). This previously unreported segregation of Si at the phase boundary may lead to better thermal stability of the intermetallic. Since the Si in this alloy was an impurity, future work could explore the potential benefits from intentional dilute Si additions to AE44.

In summary, using APT, we were able to identify the chemistry and origin of Mn precipitate formation in α-Mg during T5 heat treatment. In the as-cast state, Ce-rich clusters in the range of 3.3 ± 0.7 nm were observed in the dendritic α-Mg, acting as heterogeneous nucleation sites for the subsequent formation of nanoscale Mn-rich precipitates in the range of 6.7 ± 0.6 nm after T5 heat treatment (250°C for 4h). These particles were identified by APT as $Al_{10}Mn_7RE_2$ instead of the previously assumed Al_8Mn_5. The lamella intermetallic $Al_{11}RE_3$ phases did not show any changes in their composition or structure after heat treatment, however, a residual amount of Mg between 5-10 at. % was detected. Already in the as-cast state, Si was observed to segregate at the interface between $Al_{11}RE_3$/α-Mg. Silicon surrounded this intermetallic phase and could have a beneficial effect on thermal stability of the intermetallic at higher temperatures. The RE composition of Ce and La varied between different lamellae. Furthermore, no clusters or precipitates were observed in the inter-dendritic α-Mg in the as-cast and T5 state, although a higher concentration of RE prevailed in these locations. This suggests that the formation of Ce-rich clusters depends mainly on the solidification kinetics and not on the concentration.

Table 1: Composition of the AE44-2 ingots used for HPDC, as measured by spark optical emission spectroscopy (OES) in mass%.

Mg	Al	La	Ce	Mn	Si
Bal.	3.69	1.23	2.63	0.18	0.024

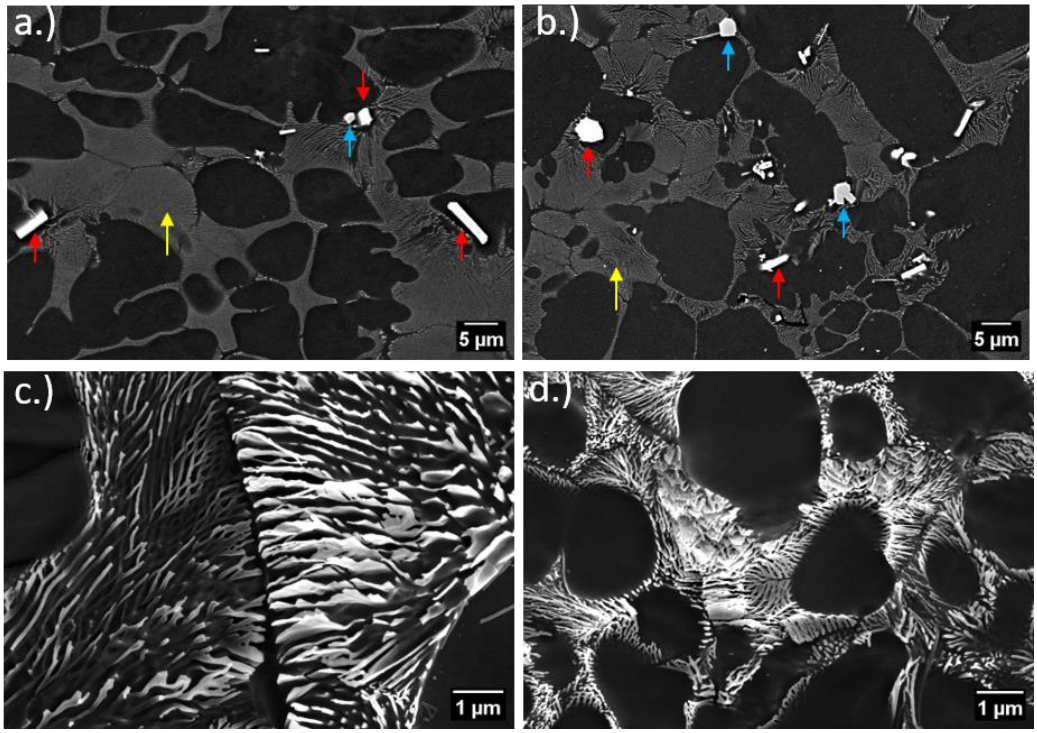

Figure 1 Comparison of microstructures in as-cast (left) and T5 heat treated (right) AE44 at two different magnifications. Top: BSE-SEM images containing α-Mg dendrites (dark), $(Al,Si)_2RE$ (red arrows), $Al_{10}Mn_7RE_2$ + Al_8Mn_4RE (blue arrows), and α-Mg + $Al_{11}RE_3$ lamellar eutectic (yellow arrows). Bottom: SE-SEM images of $Al_{11}RE_3$ lamellae after removing α-Mg by deep etching.

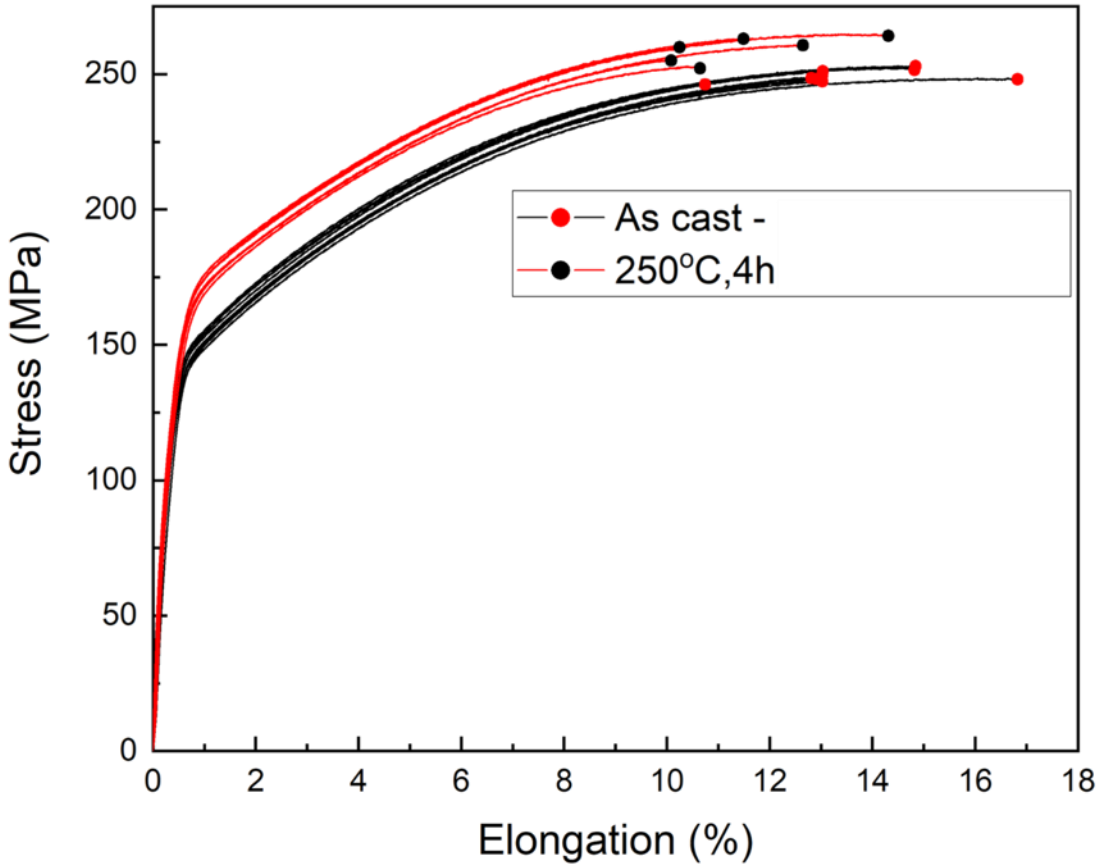

Figure 2: Tensile test curves of AE44-2 as cast and after a T5 heat treatment at room temperature.

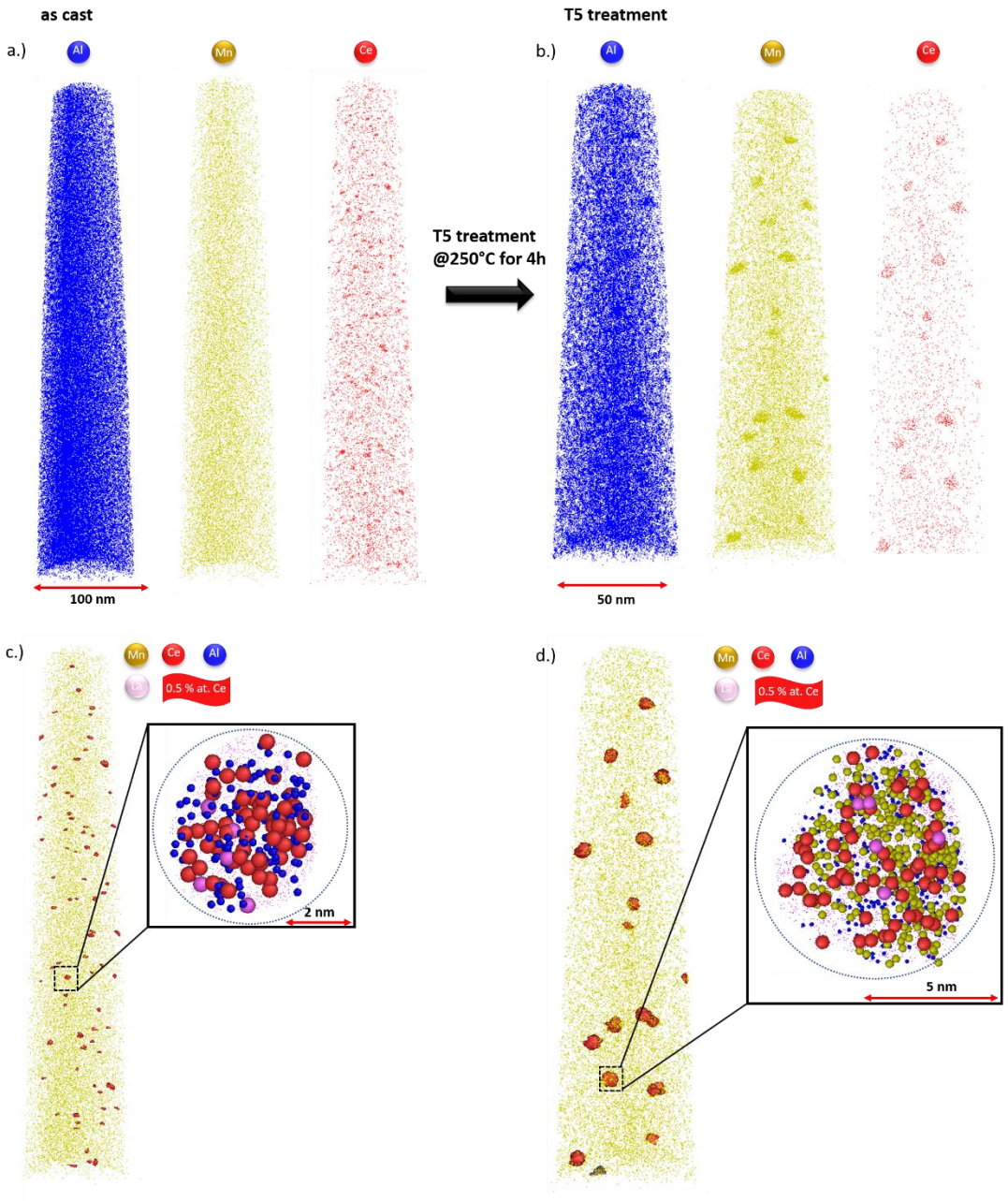

Figure 3: Individual elemental maps of the reconstructed volume of aluminum (blue), manganese (yellow) and cerium (red) in the as-cast state on the left and after a T5 heat treatment on the right. Iso-concentration plots with 0.5 at-% Ce were used to visualize the solute-rich clusters in the as cast sample and the precipitates after T5 heat treatment.

Table 2 Chemical composition of the Ce-rich clusters in the as-cast state and the Mn-rich particles after the T5 heat treatment in at. %.

	as-cast	**T5**
Mg	92.30	80.81
Al	5.50	9.88
Ce	1.98	2.09
La	0.17	0.08
Mn	0.05	7.15

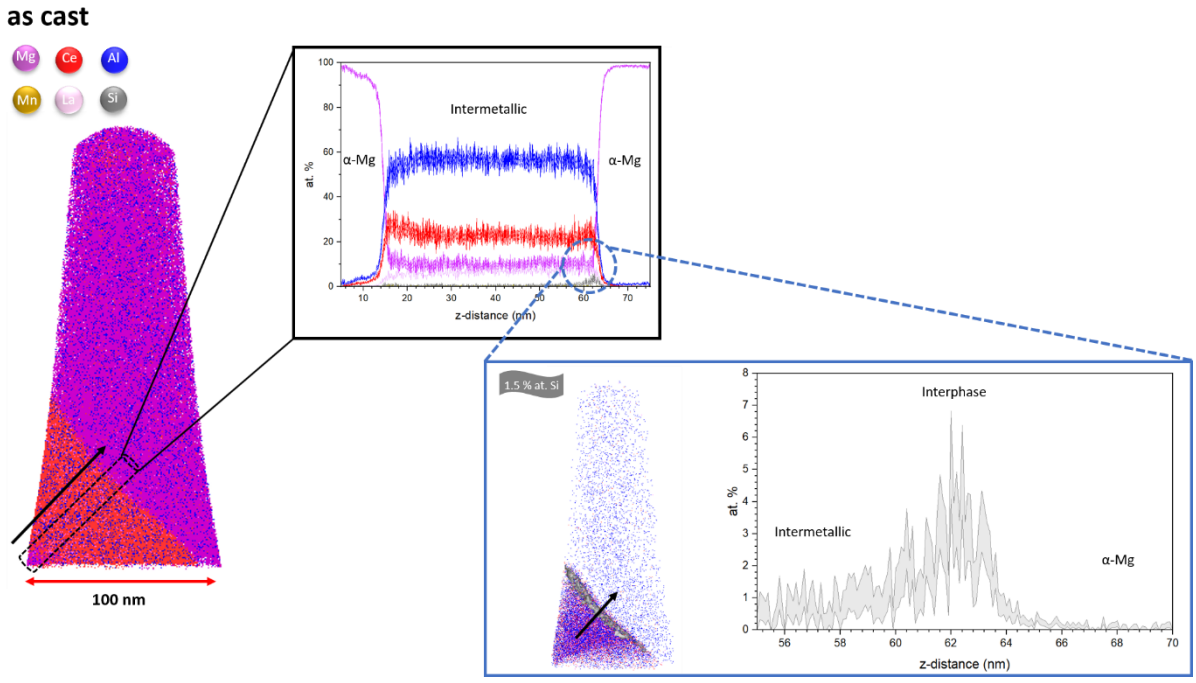

Figure 4: APT measurement of the inter-dendritic region in the as cast state containing the lamellar $Al_{11}RE_3$ phase

Table 3: Chemical composition of the $Al_{11}RE_3$ phase in the as-cast and T5 conditions in at. %.

	as-cast	T5 top	T5 bottom
Al	62.24	68.12	65.12
Ce	21.99	13.04	27.02
Mg	9.77	7.26	7.44
La	5.99	11.56	0.39
Mn	0.01	0.02	0.03

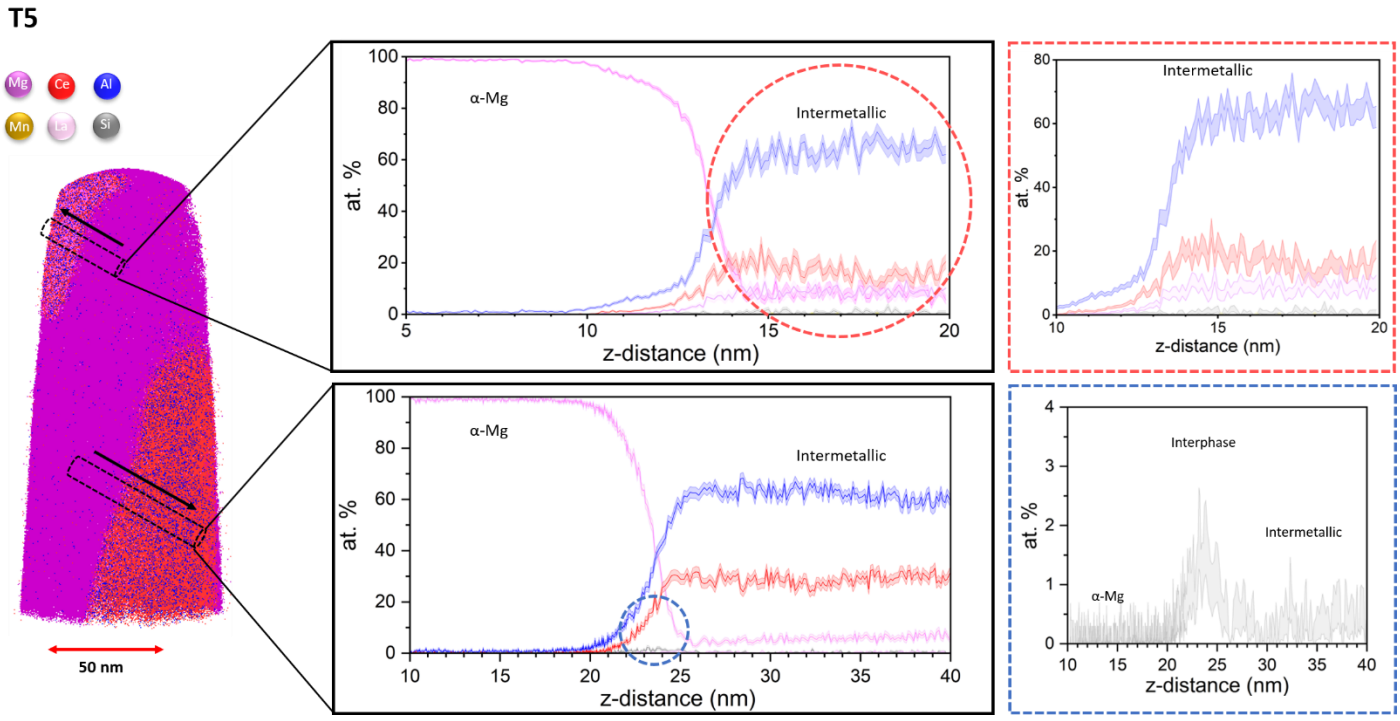

Figure 5: APT measurement of the inter-dendritic region after T5 heat treatment containing two $Al_{11}RE_3$ lamellae.

Table 4: Comparison of the composition of α-Mg in the dendritic and inter-dendritic region in the as-cast state in at. %.

	dendritic	**inter-dendritic**
Mg	98.847	98.311
Al	1.049	1.467
RE	0.017	0.073
Mn	0.025	0.020
Si	0.062	0.129

Declaration of Competing Interest

The authors declare that they have no known competing financial interest or personal relationships that could have appeared to influence the work reported in this paper.

Acknowledgments

IM & BG are grateful for funding from the ERC – SHINE (771602). TS, IM, BG are grateful for funding from the DFG through the award of the Leibniz Prize 2020. CG is grateful for funding from the EPSRC Future LiME Hub (EP/N007638/1). Uwe Tezins, Andreas Sturm and Christian Broß are acknowledged for their support to the FIB & APT facilities at MPIE.

Graphical abstract

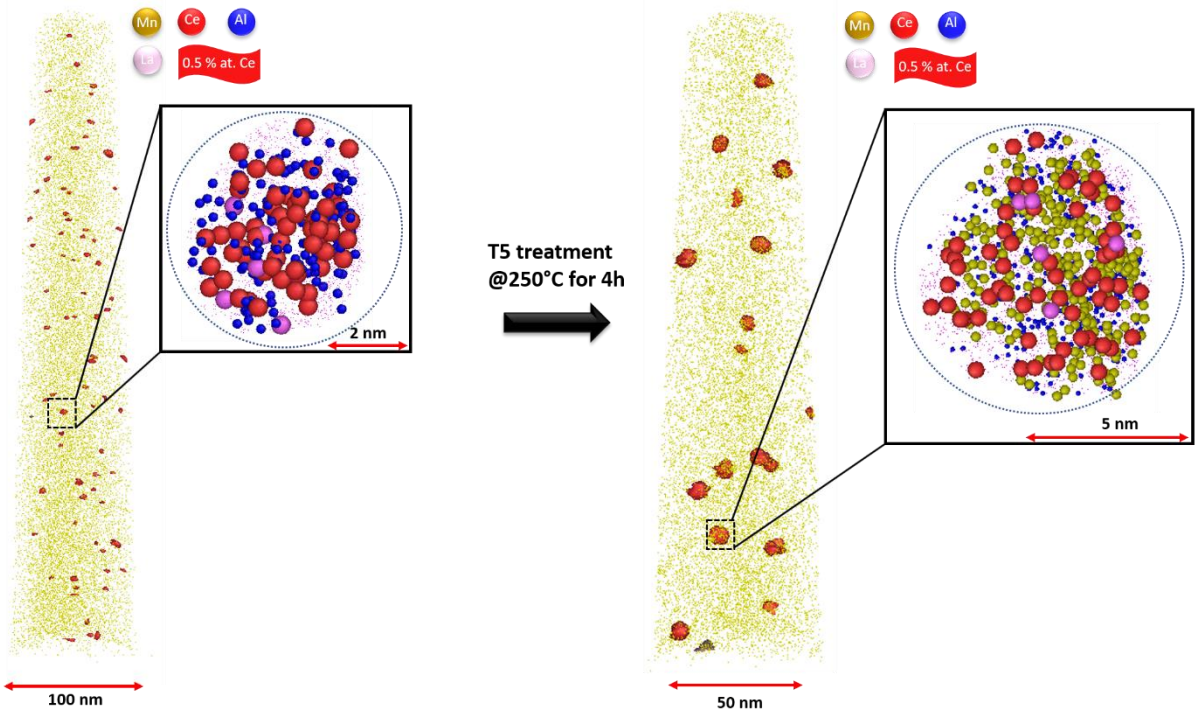

References

[1] N.E. Prasad, R.J.H. Wanhill, Aerospace Materials and Material Technologies, Springer, 2017.

[2] G. Arruebarrena, I. Hurtado, J. Väinölä, C. Cingi, S. Dévényi, J. Townsend, S. Mahmood, A. Wendt, K. Weiss, A. Ben-Dov, Development of Investment-Casting Process of Mg-Alloys for Aerospace Applications, Adv. Eng. Mater. 9 (2007) 751–756.

[3] I.J. Polmear, J.-F. Nie, M. Qian, D. StJohn, Light alloys: metallurgy of the light metals, Fifth edition, Butterworth-Heinemann, an imprint of Elsevier, Oxford, 2017.

[4] M. Easton, A. Beer, M. Barnett, C. Davies, G. Dunlop, Y. Durandet, S. Blacket, T. Hilditch, P. Beggs, Magnesium alloy applications in automotive structures, JOM. 60 (2008) 57–62.

[5] K.U. Kainer, Magnesium alloys and technology, DGM, Weinheim, 2010.

[6] S. Zhu, M.A. Easton, T.B. Abbott, J.-F. Nie, M.S. Dargusch, N. Hort, M.A. Gibson, Evaluation of Magnesium Die-Casting Alloys for Elevated Temperature Applications: Microstructure, Tensile Properties, and Creep Resistance, Metall. Mater. Trans. A. 46 (2015) 3543–3554.

[7] A.A. Luo, Recent magnesium alloy development for elevated temperature applications, Int. Mater. Rev. 49 (2004) 13–30.

[8] M. Pekguleryuz, M. Celikin, Creep resistance in magnesium alloys, Int. Mater. Rev. 55 (2010) 197–217.

[9] K.E. Nelson, Magneisum Die Casting Alloys, (1970).

[10] T.Kr. Aune, T.J. Ruden, High Temperature Properties of Magnesium Die Casting Alloys, in: 1992: p. 920070.

[11] B.R. Powell, V. Rezhets, M.P. Balogh, R.A. Waldo, Microstructure and creep behavior in AE42 magnesium die-casting alloy, JOM. 54 (2002) 34–38.

[12] P. Bakke, K. Pettersen, H. Westengen, Enhanced ductility and strength through RE addition to magnesium die casting alloys, in: 2003: pp. 171–176.

[13] P. Bakke, H. Westengen, S. Sannes, D. Albright, Powertrain Components - Opportunities for the Die Cast AE Family of Alloys, in: 2004: pp. 2004-01–0655.

[14] S.M. Zhu, M.A. Gibson, M.A. Easton, J.F. Nie, The relationship between microstructure and creep resistance in die-cast magnesium–rare earth alloys, Scr. Mater. 63 (2010) 698–703.

[15] L.L. Rokhlin, Magnesium Alloys Containing Rare Earth Metals: Structure and Properties, 0 ed., CRC Press, 2003.

[16] P. Bakke, H. Westengen, The Role of Rare Earth Elements in Structure and Property Control of Magnesium Die Casting Alloys, in: S.N. Mathaudhu, A.A. Luo, N.R. Neelameggham, E.A. Nyberg, W.H. Sillekens (Eds.), Essent. Read. Magnes. Technol., Springer International Publishing, Cham, 2016: pp. 313–318.

[17] Y.D. Huang, H. Dieringa, N. Hort, P. Maier, K.U. Kainer, Y.L. Liu, Evolution of microstructure and hardness of AE42 alloy after heat treatments, J. Alloys Compd. 463 (2008) 238–245.

[18] R.W. McCallum, L. Lewis, R. Skomski, M.J. Kramer, I.E. Anderson, Practical Aspects of Modern and Future Permanent Magnets, Annu. Rev. Mater. Res. 44 (2014) 451–477.

[19] Y.Z. Du, X.G. Qiao, M.Y. Zheng, K. Wu, S.W. Xu, Development of high-strength, low-cost wrought Mg–2.5mass% Zn alloy through micro-alloying with Ca and La, Mater. Des. 85 (2015) 549–557.

[20] S. Lun Sin, D. Dubé, R. Tremblay, Characterization of Al–Mn particles in AZ91D investment castings, Mater. Charact. 58 (2007) 989–996.

[21] J.F. Nie, B.C. Muddle, Characterisation of strengthening precipitate phases in a Mg–Y–Nd alloy, Acta Mater. 48 (2000) 1691–1703.

[22] L.Y. Wei, G.L. Dunlop, H. Westengen, Age hardening and precipitation in a cast magnesium-rare-earth alloy, J. Mater. Sci. 31 (1996) 387–397.

[23] S. Celotto, TEM study of continuous precipitation in Mg–9 wt%Al–1 wt%Zn alloy, Acta Mater. 48 (2000) 1775–1787.

[24] C.R. Hutchinson, J.F. Nie, S. Gorsse, Modeling the precipitation processes and strengthening mechanisms in a Mg-Al-(Zn) AZ91 alloy, Metall. Mater. Trans. A. 36 (2005) 2093–2105.

[25] J.-F. Nie, Precipitation and Hardening in Magnesium Alloys, Metall. Mater. Trans. A. 43 (2012) 3891–3939.

[26] L.Y. Wei, G.L. Dunlop, H. Westengen, Precipitation Hardening of Mg-Zn and Mg-Zn-RE alloys, Metall. Mater. Trans. A. 26 (1995) 1705–1716.

[27] E. Dogan, S. Wang, M.W. Vaughan, I. Karaman, Dynamic precipitation in Mg-3Al-1Zn alloy during different plastic deformation modes, Acta Mater. 116 (2016) 1–13.

[28] N. Su, Y. Wu, Q. Deng, Z. Chang, Q. Wu, Y. Xue, K. Yang, Q. Chen, L. Peng, Synergic effects of Gd and Y contents on the age-hardening response and elevated-temperature mechanical properties of extruded Mg–Gd(-Y)-Zn-Mn alloys, Mater. Sci. Eng. A. 810 (2021) 141019.

[29] J.F. Nie, K. Oh-ishi, X. Gao, K. Hono, Solute segregation and precipitation in a creep-resistant Mg–Gd–Zn alloy, Acta Mater. 56 (2008) 6061–6076.

[30] N. Stanford, D. Atwell, The Effect of Mn-rich Precipitates on the Strength of AZ31 Extrudates, Metall. Mater. Trans. A. 44 (2013) 4830–4843.

[31] A. Suzuki, N.D. Saddock, J.R. TerBush, B.R. Powell, J.W. Jones, T.M. Pollock, Precipitation Strengthening of a Mg-Al-Ca–Based AXJ530 Die-cast Alloy, Metall. Mater. Trans. A. 39 (2008) 696–702.

[32] R.N. Lumley, R.G. O'Donnell, D.R. Gunasegaram, M. Givord, Heat Treatment of High-Pressure Die Castings, Metall. Mater. Trans. A. 38 (2007) 2564–2574.

[33] S.M. Zhu, T.B. Abbott, M.A. Gibson, J.F. Nie, M.A. Easton, Age hardening in die-cast Mg–Al–RE alloys due to minor Mn additions, Mater. Sci. Eng. A. 656 (2016) 34–38.

[34] S.M. Zhu, T.B. Abbott, M.A. Gibson, J.F. Nie, M.A. Easton, The influence of minor Mn additions on creep resistance of die-cast Mg–Al–RE alloys, Mater. Sci. Eng. A. 682 (2017) 535–541.

[35] S. Zhu, T.B. Abbott, J.-F. Nie, H.Q. Ang, D. Qiu, K. Nogita, M.A. Easton, Re-evaluation of the mechanical properties and creep resistance of commercial magnesium die-casting alloy AE44, J. Magnes. Alloys. 9 (2021) 1537–1545.

[36] Q. Yang, K. Guan, B. Li, S. Lv, F. Meng, W. Sun, Y. Zhang, X. Liu, J. Meng, Microstructural characterizations on Mn-containing intermetallic phases in a high-pressure die-casting Mg–4Al–4RE–0.3Mn alloy, Mater. Charact. 132 (2017) 381–387.

[37] Y. Li, J. Wang, H. Ma, Z. Zhen, Y. Liu, H. Zhang, P. Jin, An investigation on the precipitates in T5 treated high vacuum die-casting AE44–2 magnesium alloy, Mater. Res. Express. 9 (2022) 020005.

[38] B. Gault, A. Chiaramonti, O. Cojocaru-Mirédin, P. Stender, R. Dubosq, C. Freysoldt, S.K. Makineni, T. Li, M. Moody, J.M. Cairney, Atom probe tomography, Nat. Rev. Methods Primer. 1 (2021) 51.

[39] S.M. Zhu, M.A. Gibson, J.F. Nie, M.A. Easton, T.B. Abbott, Microstructural analysis of the creep resistance of die-cast Mg–4Al–2RE alloy, Scr. Mater. 58 (2008) 477–480.

[40] S.M. Zhu, J.F. Nie, M.A. Gibson, M.A. Easton, P. Bakke, Microstructure and Creep Behavior of High-Pressure Die-Cast Magnesium Alloy AE44, Metall. Mater. Trans. A. 43 (2012) 4137–4144.

[41] T. Rzychoń, A. Kiełbus, J. Cwajna, J. Mizera, Microstructural stability and creep properties of die casting Mg–4Al–4RE magnesium alloy, Mater. Charact. 60 (2009) 1107–1113.

[42] K.A. Gschneidner, F.W. Calderwood, The Al−Ce (Aluminum-Cerium) system, Bull. Alloy Phase Diagr. 9 (1988) 669–672.

[43] G. Pettersen, H. Westengen, R. Høier, O. Lohne, Microstructure of a pressure die cast magnesium—4wt.% aluminium alloy modified with rare earth additions, Mater. Sci. Eng. A. 207 (1996) 115–120.

[44] K. Thompson, D. Lawrence, D.J. Larson, J.D. Olson, T.F. Kelly, B. Gorman, In situ site-specific specimen preparation for atom probe tomography, Ultramicroscopy. 107 (2007) 131–139.

[45] L. Lilensten, B. Gault, New approach for FIB-preparation of atom probe specimens for aluminum alloys, PLOS ONE. 15 (2020) e0231179.

[46] D. Blavette, F. Vurpillot, P. Pareige, A. Menand, A model accounting for spatial overlaps in 3D atom-probe microscopy, Ultramicroscopy. 89 (2001) 145–153.

[47] S. Lamm, D. Matschkal, M. Göken, P. Felfer, Impact of Mn on the precipitate structure and creep resistance of Ca containing magnesium alloys, Mater. Sci. Eng. A. 761 (2019) 137964.

[48] T. Rzychoń, A. Kiełbus, L. Lityńska-Dobrzyńska, Microstructure, microstructural stability and mechanical properties of sand-cast Mg–4Al–4RE alloy, Mater. Charact. 83 (2013) 21–34.

[49] H. Xue, W. Xie, S. Liu, Y. Zhou, J. Peng, H. Pan, D. Zhang, F. Pan, The formation mechanism of Al-RE tubular phase in AZ80-Ce magnesium alloy by La doping, J. Mater. Res. Technol. 18 (2022) 1105–1114.

[50] J. Zhang, D. Zhang, Z. Tian, J. Wang, K. Liu, H. Lu, D. Tang, J. Meng, Microstructures, tensile properties and corrosion behavior of die-cast Mg–4Al-based alloys containing La and/or Ce, Mater. Sci. Eng. A. 489 (2008) 113–119.